



**3D numerical modeling of free surface flow with air
entrainment. Complementary spillway of Salamonde.**

Extended Abstract

Eddy Nelson dos Reis Pereira

(eddy.pereira@tecnico.ulisboa.pt)

Supervisor

António Alberto do Nascimento Pinheiro

June 2016

1. Introduction

CFD (Computational Fluid Dynamics) models are very useful for the majority of the industry, as they allow to develop alternative solutions in a faster and economical way. These models can also significantly reduce the use of physical models, and avoid some scale effects that physical models cannot overcome. From this point of view, CFD models may be regarded as a complementary tool for a more efficient design procedure.

A key advantage of using CFDs is the possibility of economically varying the geometry and other features for a given prototype. This may improve the solutions that, in the end, may be tested in physical models, saving time and money.

In rapidly varied regimes occurring in complex geometry prototypes, 1-D and 2-D numerical models are limited for the representation of flow characteristics, compared to the potential of CFD 3-D models that allow to simulate, with high precision, turbulence effects associated for this type of regime.

2. Objectives

This dissertation intends to assess the numerical capabilities of air entrainment and sediment transport simulation of the commercial CFD FLOW-3D® applied to the complementary spillway of Salomonde dam, departing from the research developed by Silva (2013) and using physical model results, respectively.

Additionally, FLOW-3D® is also used to study alternative outlet structures for the spillway, analyzing the corresponding jets and the respective scour holes.

3. Fundamental theory

3.1. Air entrainment and scale effects

According to Chanson (2001), scale effect is the discrepancy between model and prototype resulting when one or more dimensionless parameters have different values in the model and prototype.

The correct physical modeling of a two-phase flow in a physical model requires a correct representation of the similarity laws.

The similitude of the behavior of a two-phase flow between two systems is guaranteed if both match the same Morton number. However, the Morton similarity between two systems guarantees correct reproduction of the air bubbles, but does not characterize the problem of shear layer for a free jet.

The air entrainment in a free surface mainly results from the development of small turbulent structures in the air-water free surface, which have the capacity to trap air carrying it to the core of the flow.

The entrance of air in the flow, through the free surface, is defined by an equilibrium condition between the turbulent kinetic energy per unit volume (turbulent energy uplift), P_t , and energy stabilizing forces, P_d . Numerically, the scalar method of the air entrainment model allows the volume entrance of air to the mixture, through the following expression:

$$\begin{cases} \delta V = 0, & \text{if } P_T < P_d \\ \delta V = C_{air} A_s \left[\frac{2(P_T - P_d)}{\rho_{mix}} \right]^{\frac{1}{2}}, & \text{if } P_T > P_d \end{cases} \quad (3.1)$$

where, ρ_{mix} define the density of the flow mixture, which is equal to the density of water, ρ_w , when only scalar method is selected.

The definition of the mixture density is determined by the implementation of density evaluation method through the following expression:

$$\rho_{mix} = F\rho_w + (1 - F)\rho_{air} \quad (3.2)$$

where F represents the volumetric fraction and ρ_{air} the air density.

The density evaluation method considers the bulking increase in the mixture, modifying the flow behaviour, when the entrained air is higher than 1-3%.

The numerical implementation of the drift-flux method considers the possibility of the air being entrained as a cloud of tiny bubbles, which not only bulk the fluid but also affect the flow in two additional ways: by adding relative velocity between the air and water, and by adding bubble form drag and inter-bubble wake drag (Hirt, 2007).

3.2. Flow-3D sediment scour formulation

FLOW-3D® sediment scour model includes several numerical formulations that can describes sediment transport behaviour, namely: drifting/settling, suspension, lifting, bed load and packing fraction processes.

Bed load (rolling, sliding and saltating) and suspension motions are numerically solved separately through the numerical definition of the saltation height layer, δ_i , and packing fraction (Flow Science, 2014; Van Rijn, 1984). Fernandez Luque, in Van Rijn (1984), measured and computed saltation characteristics for three equivalent roughness of Nikuradse cases, k_s/d_{50} , and concluded that the saltation layer increase for smaller values. Van Rijn (1984) also defined that the saltation height layer is equivalent to the thickness of the bed load layer:

$$\frac{\delta_i}{d_{50}} = 0.3d_{*,i}^{0.7} \left(\frac{\theta_i}{\theta_{cr}} - 1 \right)^{0.5} \quad (3.3)$$

The bed load layer concentration (also called by packing fraction), f_b , is defined by the following expression:

$$f_{b,i} = 0.18 \frac{f_{s,crit}}{d_*} \left(\frac{\theta_i}{\theta_{cr}} - 1 \right) \quad (3.4)$$

where, $f_{s,crit}$, is the maximum bed load concentration, called by maximum packing fraction in FLOW-3D®, d_* , is the dimensionless diameter, θ_{cr} , is the dimensionless Shields parameter, and θ_i is the Shields effectiveness parameter.

The Shields parameter can be computed by Soulsby-Whitehouse (1997) formulation or manually by the user. Slope and hiding-exposure formulations can also be optionally implemented to the numerical Shields formulation.

In FLOW-3D®, settling, lifting, and bed load velocity motions are defined, respectively, by the Soulsby (1997), Winterwerp (1992) and Meyer-Peter-Müller (1948) formulations, through the following expressions:

$$u_{settling,i} = \frac{v_f}{d_i} [(10.36^2 + 1.049d_*^3)^{0.5} - 10.36] \quad (3.5)$$

$$u_{lift,i} = \alpha n_s d_{*,i}^{0.3} (\theta_i - \theta_{cr})^{1.5} \sqrt{g d_i (s - 1)} \quad (3.6)$$

$$u_{bedload,i} = \frac{q_{b,i}}{\delta_i f_{b,i}}$$

$$\phi_i = \beta_i (\theta_i - \theta_{cr,i})^{1/3} \quad (3.7)$$

$$q_{b,i} = \phi_i \left[g \left(\frac{\rho_{s,i} - \rho_f}{\rho_f} \right) d_i^3 \right]^{1/2}$$

in which α and β are the lift and bed load calibration factors, respectively, and ϕ_i and $q_{b,i}$ are the dimensionless and volumetric bedload transport rate.

4. Case study

The present case study results from Silva (2013) CFD study of the complementary spillway of Salamonde dam, which analysed FLOW-3D® model capacities to simulate several flow discharges into this bended complex geometry.

The flow characteristics for the original spillway design discharge (1233m³/s) are evaluated at the present case study, without and with implementing the air entrainment model.

Three different alternatives outlet structures (Figure 4.2) are also simulated with the air entrainment activation model. All these alternatives, consider the two spans along all the tunnel structure (Figure 4.1 (b)), whereas the original geometry considered the reunion of the the two spans at the end of the bend.

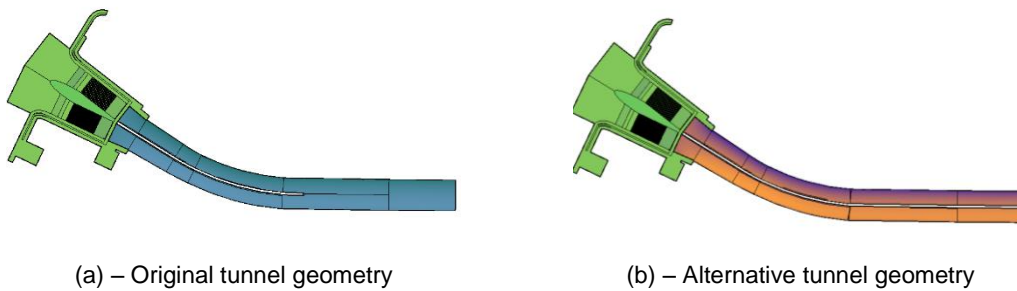


Figure 4.1 – Tunnel geometries.

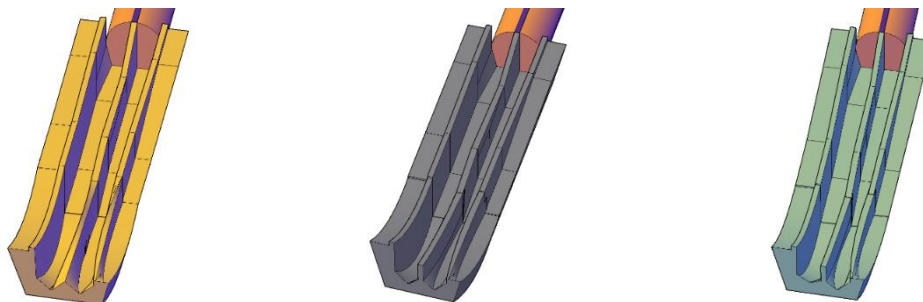
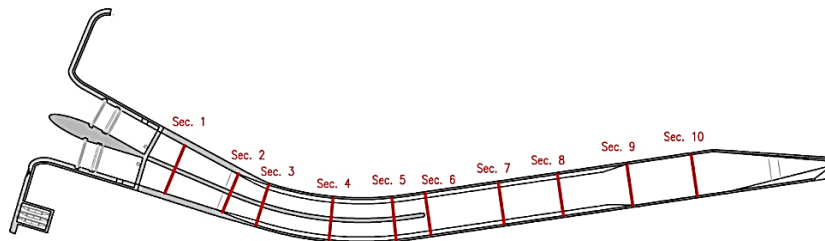


Figure 4.2 – Alternatives outlet structures.

Aqualogus (2011) presented the flow characteristics occurring in the original complementary spillway, obtained with a 1-D model, in ten reference sections (Figure 4.3).



(a) - Plan view

Figure 4.3 – Reference sections.

Numerical specifications between Silva (2013), Aqualogus (2011) and the present model are presented in Table 4.1.

Table 4.1 - Numerical specifications that were applied to the studies of the complementary spillway of Salomonde dam.

| Model | Time results (s) | Numerical model | Cell Size (m) | TLEN (m) |
|------------------|------------------|-----------------|---------------|----------------------|
| Aqualogus (2011) | - | 1-D | - | - |
| Silva (2013) | 70 | 3-D (FLOW-3D®) | 0,25 | 0,4 |
| Present study | 150 | 3-D (FLOW-3D®) | 0,50 | Dynamically computed |

Scour holes are modelled for a plunge pool with an elevation of 209,30 m and with a flat sediment bottom composed by one layer, characterized with grains size of 1,10 m. Physical processes of a scour hole development by water jet impingement differ significantly to bed load transport processes. Meyer-Peter-Müller numerical formulation is not adjusted to the grain size case and does not represent appropriately scour hole processes. Thus, bed load transport numerical formulation was not activated.

5. Air entrainment results

5.1. Flow discharge

In order to assess the influence of turbulence models and air entrainment formulations into the water-air flow discharge capacity, several simulations were performed (Table 5.1).

Table 5.1 – Air entrainment simulation tests.

| | Turbulence | | Air entrainment formulations | | | | |
|---------------------|------------|----------------------|------------------------------|--------------------|------------|-------------------|-----------------|
| | Model | TLEN (m) | Scalar | Density evaluation | Drift-Flux | Adiabatic bubbles | Surface tension |
| SV 1 ⁽¹⁾ | RNG k-e | D.Compt ² | x | x | x | - | - |
| SV 2.1 | RNG k-e | 0,5 | x | x | x | - | - |
| SV 2.2 | RNG k-e | D.Compt | x | x | x | - | - |
| SV 3 | RNG k-e | D.Compt | x | x | x | x | - |
| SV 4 | RNG k-e | D.Compt | x | x | x | x | 0,073 |
| SV 5 | LES | | x | x | x | x | 0,073 |

Water-air flow discharge capacities, and original and alternative spillways rating curves for SV4 parameters simulation are presented on the Table 5.2 and Figure 5.1, respectively.

Table 5.2 – Averaged water-air flow discharge capacity in a control section in the downstream limit of the tunnel structure.

| | Air entrained volume flow rate (m ³ /s) | Liquid volume flow rate (m ³ /s) |
|--------------|--|---|
| SV1 | 128 | 1306 |
| SV2.1 | 255 | 1427 |
| SV2.2 | 248 | 1418 |
| SV3 | 128 | 1302 |
| SV4 | 127 | 1302 |
| SV5 | 5,0 | 1185 |
| Silva (2013) | 0 | 1206 |
| Aqualogus | - | 1233 |

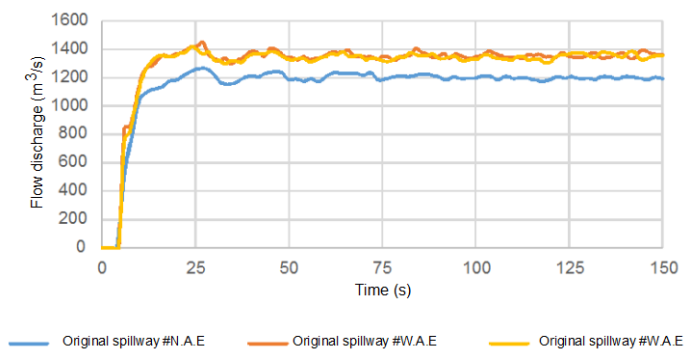


Figure 5.1 – Original and alternative tunnel rating curve.

(1) – Cell size: 1.00 m

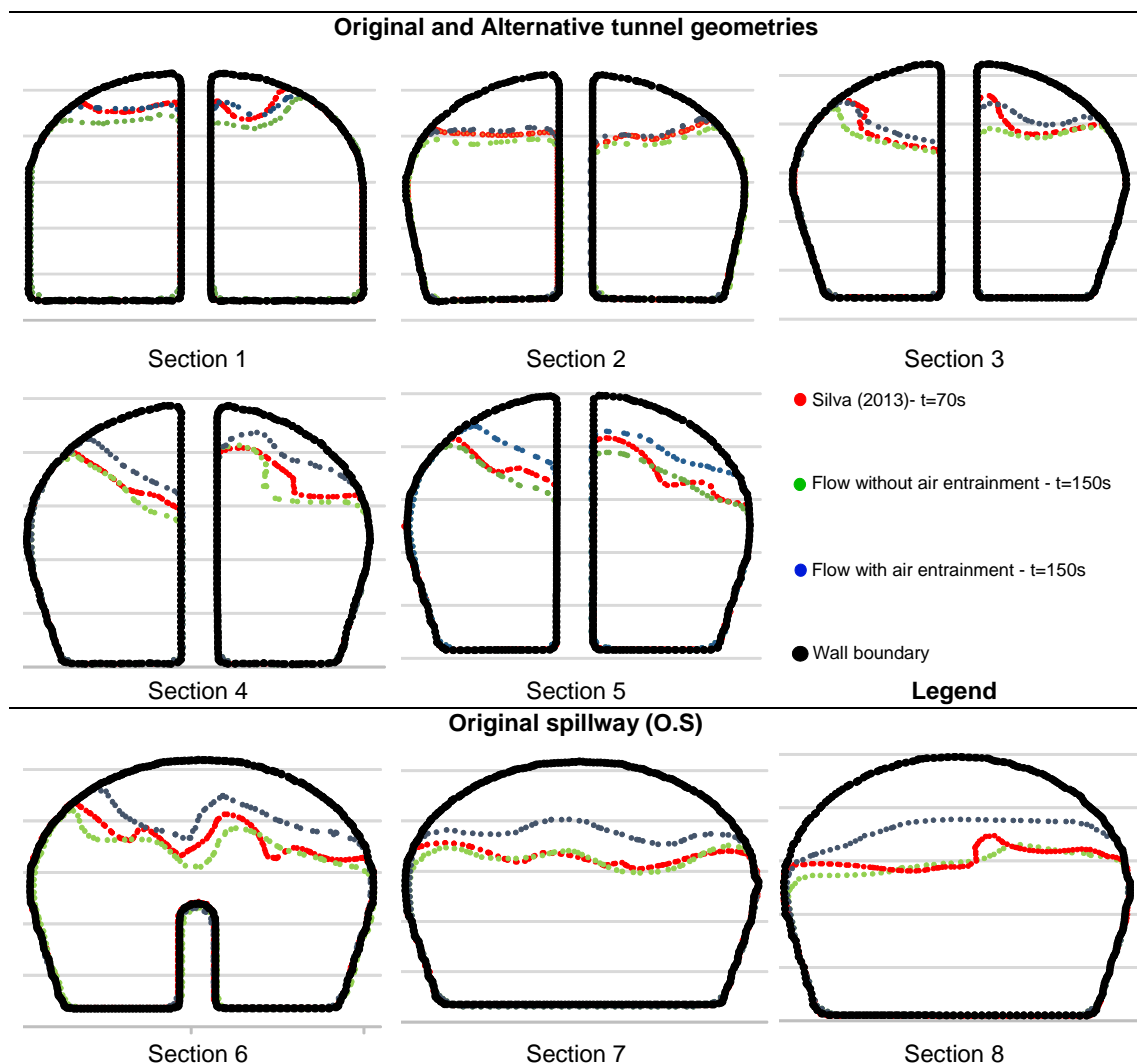
(2) - D. Compt: Dynamically Computed

It is important to notice that all the two-phase flow simulations over predicted more or less significantly the flow discharge capacity (SV5 LES simulation is an exception), in comparison the Aqualogus (2011) project design and Silva (2013) numerical model.

Silva (2013) results underestimated the flow discharge in 2,2% in comparison to the project design. The numerical model is reproduced from the prototype scale, and it is observed that the definition of superficial tension has a residual influence on the air entrainment. It is also important to notice that the activation of the adiabatic bubbles have a major importance to control the effect of the pressure gradient for extremely accelerated regime.

An increase of +8% for the discharge capacity was observed for the SV4 simulation, in comparison to Silva (2013) results. Thus, SV4 parameters were adopted to proceed for the validation of the main flow characteristics results.

Figure 5.2 shows the flow cross sections for the reference sections 1 to 8, for the original and alternative tunnel geometries.



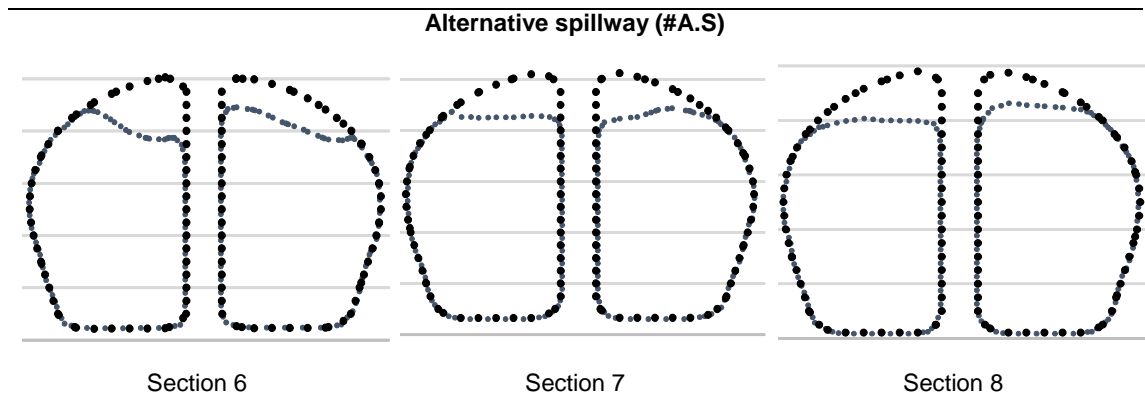


Figure 5.2 – Flow depths in the original and alternative tunnel geometries.

Table 5.3 presents the reference sections flow areas, for the original and alternatives tunnel geometries, for the present numerical model (SV4).

Table 5.3 - Flow areas (m²).

| Spillway part | Tunnel | | | | | | | | Outlet | |
|---------------------------------------|-------------|-------------|--------------|--------------|--------------|--------------|--------------|--------------|--------------|--------------|
| Section | 1 | 2 | 3 | 4 | 5 | 6 | 7 | 8 | 9 | 10 |
| Original spillway #N.A.E ³ | 115,3 | 88,2 | 78,3 | 81,9 | 64,9 | 63,3 | 59,2 | 58,1 | 56,8 | 59,1 |
| Original spillway #W.A.E ⁴ | 118,1 | 93,0 | 83,4 | 90,9 | 73,4 | 73,9 | 68,7 | 69,8 | 67,2 | 69,2 |
| Diff. (%) | +2,4 | +5,5 | +6,5 | +11,0 | +13,0 | +16,8 | +15,9 | +20,2 | +18,3 | +17,0 |
| Alternative tunnel | | | ⁵ | | | 74,04 | 73,59 | 74,93 | - | - |
| Alternatives outlet | - | - | - | - | - | - | - | - | 79,5 | 80,9 |

For a comparative analysis reason, were made simulations with 150 s to obtain a steady flow for the design discharge conditions, by the fact that an unsteady turbulent flow regime was verified from Silva (2013). Increasing flow areas over downstream sections, due to higher air concentrations, were verified. It is also observed that an elevated difference occurs at the last section of the tunnel structure, due to higher levels of turbulence, air concentrations and, consequently, bulking mixture effects.

It was expected that higher values came from to the outlet structure, instead, flow contraction was found that contributed to an acceleration of the jet flow, and this alters the normal aerated flow regime to the bulk mixture.

³ - #N.A.E – No Air Entrainment modeling

⁴ - #W.A.E – With Air Entrainment modeling

⁵ - These values are the same to the *Original spillway #W.A.E* values for the reason that the first five section configurations are the same (flow discharge in two spans).

5.2. Velocities

Tables 5.4, 5.5 and 5.6 presents the average and maximum flow velocities of the original, alternative tunnel, and outlet structures.

Table 5.4 – Maximum flow velocities (m/s) in the original spillway.

| Spillway part | Tunnel | | | | | | | | Outlet | |
|---------------|--------------------|-------|-------|-------|-------|-------|-------|-------|--------|-------|
| Section | 1 | 2 | 3 | 4 | 5 | 6 | 7 | 8 | 9 | 10 |
| Model | Maximum velocities | | | | | | | | | |
| #N.A.E | 20,31 | 22,62 | 23,66 | 24,25 | 24,65 | 25,26 | 25,74 | 26,17 | 24,80 | 24,64 |
| #W.A.E | 20,92 | 22,27 | 23,60 | 24,17 | 24,60 | 25,24 | 25,60 | 26,37 | 24,49 | 24,42 |
| Diff. (%) | +3,00 | -1,55 | -0,25 | -0,33 | -0,20 | -0,08 | -0,54 | +0,76 | -1,25 | -0,89 |

Table 5.5 – Mean flow velocities in the original spillway.

| Spillway part | Tunnel | | | | | | | | Outlet | |
|------------------|---------------------|--------|--------|--------|-------|-------|-------|-------|--------|-------|
| Section | 1 | 2 | 3 | 4 | 5 | 6 | 7 | 8 | 9 | 10 |
| Model | Averaged velocities | | | | | | | | | |
| Aqualogus (2011) | 20,59 | 23,34 | 23,51 | 24,01 | 24,50 | 24,62 | 24,83 | 25,41 | 25,88 | 26,36 |
| Silva (2013) | 18,30 | 19,45 | 21,07 | 21,50 | 21,69 | 21,88 | 22,42 | 22,86 | 23,59 | 23,88 |
| #N.A.E | 14,89' | 15,51' | 16,88' | 16,97' | 21,22 | 21,04 | 21,96 | 22,28 | 22,67 | 22,82 |
| #W.A.E | 14,71' | 15,07' | 16,66' | 16,19' | 20,57 | 20,31 | 21,17 | 21,44 | 21,98 | 22,00 |
| Diff. (%) | -1,21 | -2,84 | -1,30 | -4,60 | -3,06 | -3,47 | -3,60 | -3,77 | -3,04 | -3,59 |

Table 5.6 - Flow velocities in the alternatives structures.

| Spillway part | Tunnel | | | Outlet | |
|------------------------|--------|-------|-------|--------|-------|
| Section | 6 | 7 | 8 | 9 | 10 |
| Mean velocity (m/s) | 19,89 | 20,29 | 20,20 | 21,37 | 21,30 |
| Maximum velocity (m/s) | 24,54 | 24,80 | 25,29 | 25,40 | 24,15 |

Figure 5.3 shows the transversal velocity field into the original and alternatives outlet structures.

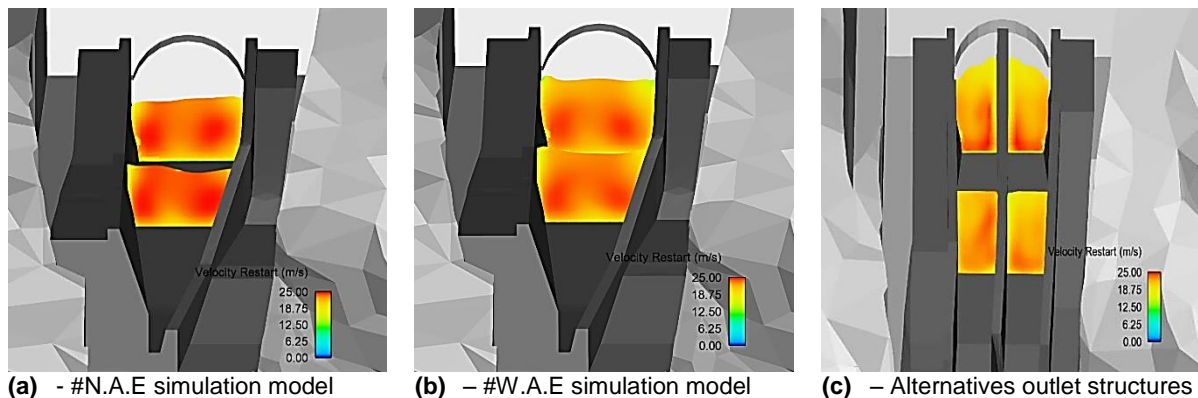


Figure 5.3 – Transversal flow velocity into the original and alternative spillway.

The obtained results show a global velocity reduction at the outlet structures. This probably occurs due to the bulking effect simulation. These results contradict the theoretical expected tendency, which suggested higher velocity values due to a lower flow resistance that occurs by water-air shear reduction.

Average flow velocities results, signalled by (*), are out of the expected range. The FlowSight® post-processing software presents a higher average errors values in mesh blocks that were not aligned to the preferential direction flow. This occurs in the first references sections, due the bended configuration of the tunnel structure into this mesh block region.

5.3. Pressure

Figure 5.4 shows the pressure diagrams from Silva (2013) and present case study models into the original outlet structure.

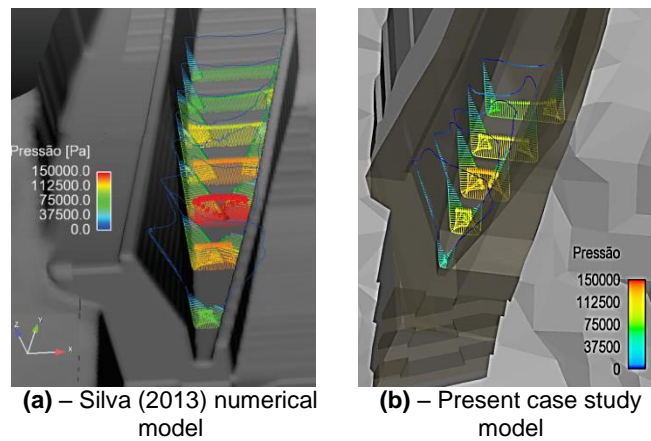


Figure 5.4 – Pressure diagrams into the original outlet structure.

An average pressure reduction of -2,7% over the convergent sidewalls was observed with air entrainment modeling. The major explanation for this results is the bulking mixture resulting for inertial forces reduction, per unit of area.

5.4. Air concentration

Comparatively to N.A.E modeling, higher TLEN values for the original outlet W.A.E were observed in section 9 and 10. This fact can be explained through the bulking mixture effect over the free surface flow, resulting to higher turbulence effect in this region, providing an increased capacity to entrained air. Overestimations of +29,1% and +25,1% for maximum TLEN values, in section 9 and 10, respectively, were observed. The air concentration, between section 5 and the outlet limit, for the original tunnel structure, is higher than the alternative one (+11,3% and +23,9%, in the left and right galleries, respectively). This fact can be explained by the higher turbulence effect resulting from the flow convergence into the original spillway, comparatively to the alternative one.

5.5. Jet flow

For the original and alternatives outlet structures, the jets configurations in the physical model, obtained by Silva (2013) and obtained in the present study are shown in Figures 5.4 and 5.5.

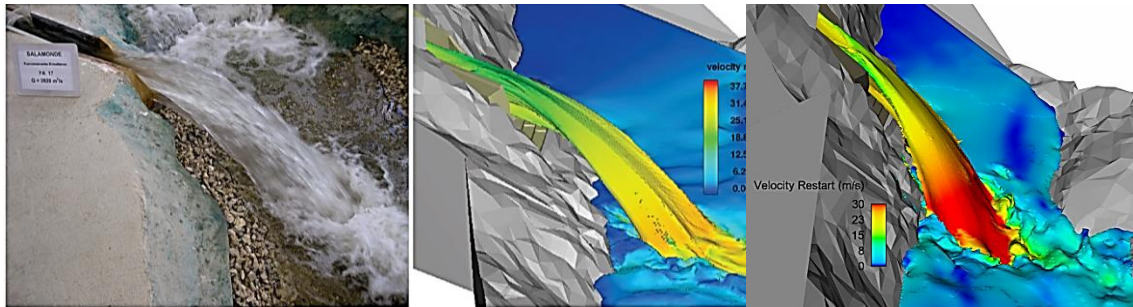
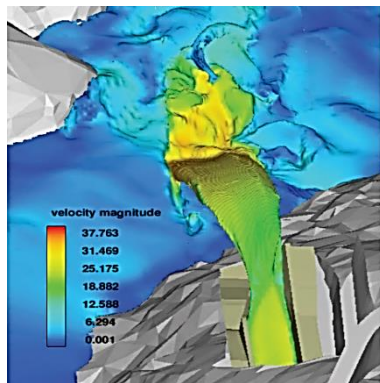
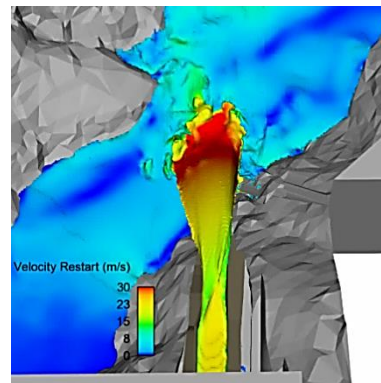


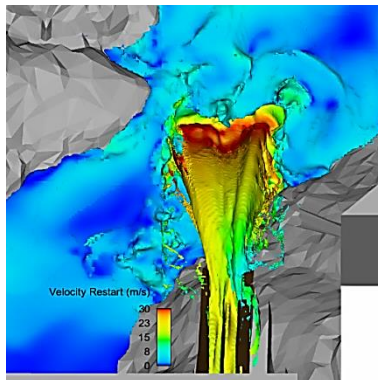
Figure 5.4 - Jet flow configurations: physical model, Silva (2013) and present study.



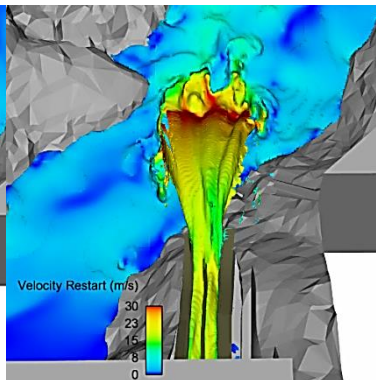
(a) - Jet flow modeling by Silva (2013) for the original outlet structure



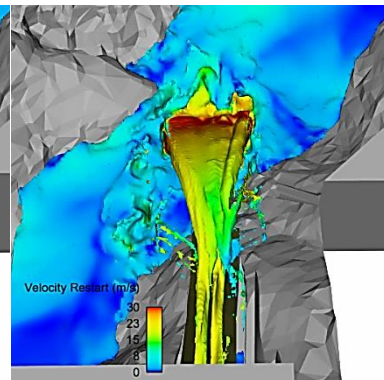
(b) - Jet flow W.A.E modeling for the original outlet structure



(c) - Jet flow W.A.E modeling for the alternative outlet structure 1



(d) - Jet flow W.A.E modeling for the alternative outlet structure 2



(e) - Jet flow W.A.E modeling for the alternative outlet structure 3

Figure 5.5 - Plan view of the jet flow configurations.

Comparatively to Silva (2013) model, in the original outlet structure a higher lateral jet flow dispersion occurred with air entrainment modeling, which was qualitatively more accurate to the physical model. By a qualitative assessment of jet impingement, it can be observed that the jet length is higher for the W.A.E simulation (Figure 5.5 (b)), comparatively to Silva model (Figure 5.5 (a)).

Table 5.7 - Free jet impingement distance results.

| Original outlet structure | | | | | Alternatives outlet structures | | |
|---------------------------|------------------|--------------|-----------|--------|--------------------------------|--------|--------|
| Physical model | AQUALOGUS (2011) | Silva (2013) | #N.A.E | #W.A.E | 1 | 2 | 3 |
| 91,0 | 72,7 | 68,4* | 56,3 | 55,9 | 68,9 | 73,4 | 68,9 |
| | | | Diff. (%) | -0,71 | +22,38 | +30,37 | +22,38 |

It is noticeable that Silva (2013) maximum impingement distance (*) presents a value higher than it really occurs, comparatively to LNEC measurement criteria, which were adopted in all the present simulations. It was also observed that the air entrainment formulations do not affect the jet length increase. The maximum jet length is significantly underestimated, comparatively to the physical model (-63%) and to Aqualogus (2011) formulation (-30%).

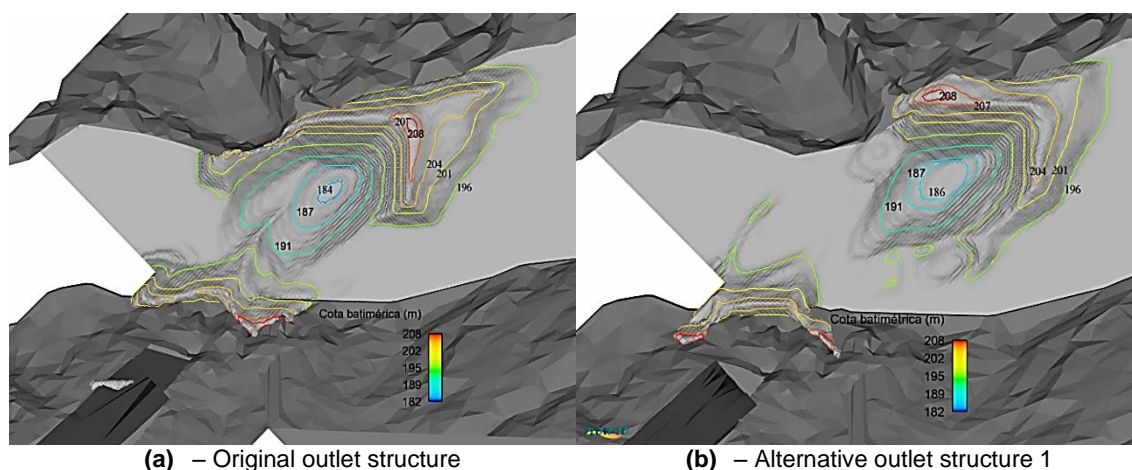
It is believed that these relative differences result from imprecisions of the physical model and numerical criteria measures. However, it is believed that the major effect results from unrepresented air bubbles scale effects in the physical model.

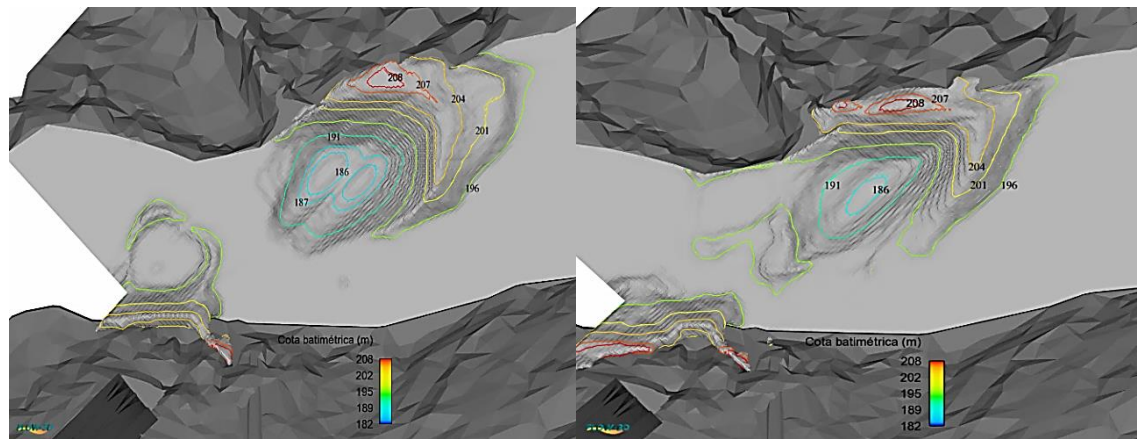
It is important to notice the CFD models capacities to test, in a simple and effective way, alternative configurations, which was verified at the present case. Indeed, the proposed alternatives outlet structures geometries clearly improve the jet impingement and lateral deflection as well in the river valley.

6. Scour hole results

The numerical modelling capabilities to represent scour holes produced by a free falling jet were assessed. Figure 6.1 shows the scour hole configurations resulting from free falling jets issued by the original and by the alternatives outlet structures. It is important to notice that the computation of bed load transport was not activated because the empirical Meyer-Peter-Müller formulation does not appear appropriate to the grain size that was considered ($D=1,10$ m). Due to processing requirements of simultaneous computation of water flow and sediment transport, the water flow simulation into all the spillway domain is carried out for mesh cells size of 1,00 m.

This fact results in free falling jets poorly represented, that are thicker due to the higher lateral dispersion. Consequently, poor free surface track and scour hole configurations are expected.





(c) – Alternative outlet structure 2 (d) – Alternative outlet structure 3

Figure 6.1 - Scour hole configurations.

Table 6.1 presents the scour holes dimensions obtained from the physical model and from the computational model.

Table 6.1 - Ridge and scour hole physical and computational results.

| Model | Scour hole | | Ridge | |
|------------------|---------------|-------------------|----------------|-------------------|
| | Max.Depth (m) | Min.Elevation (m) | Max.Height (m) | Max.Elevation (m) |
| Physical | -13 | 182 | 13 | 208 |
| Original | -11,21 | 183,79 | 14,20 | 209,20 |
| Diff. (%) | -16,0 | | +9,0 | |
| Alternative 1 | -10,03 | 184,97 | 13,14 | 208,14 |
| Alternative 2 | -10,05 | 184,95 | 13,18 | 208,18 |
| Alternative 3 | -9,99 | 185,01 | 13,37 | 208,97 |

The maximum depth of the scour hole and ridge height differences, for the original structure, were determined between the physical and computational models. It is believed that the differences result from grain size scale effects, which are affected by some parameters definitions, such as the angle of repose and the Nikuradse roughness. In fact, for the considered prototype granulometry ($D=1,10$ m), an angle of repose of 37° was defined, which is expected to be smaller in the physical model, due to the grain size scale reduction ($D=22$ mm). It is also believed that the scale effects contribute to a higher ridge elevation in the prototype, resulting a higher slope development.

7. Conclusions

Good validation results were obtained in Silva (2013) FLOW-3D® computational model, accurately representing the free surface flow along the complementary spillway of Salomonde dam. This author concluded that, for lower discharges, the computed flow depths were underestimated comparatively to the physical model. Flow characteristics for the design discharge were not measured in the physical model. Thus, flow depths were analysed by comparison between design and computational values, which allowed concluding the latter ones were higher (average difference of around 10% forward the section 3).

For the design discharge, the air entrainment computational model overestimated the flow areas due the increase of air concentration for downstream sections (from +2,4%, in section 1, to +20%, in section 8), that contribute to increasing bulking effects, revealing the expected theoretical tendency. However, some

conclusions could not be drawn, for the simple reason that the computational model represented the prototype, and Morton's scale effects could not be produced in the physical model.

It was verified that flow discharge capacity increased with air entrainment modeling, which results in a difference of 18% comparatively to Silva (2013) model. But still, the adiabatic bubbles model implementation control the pressure-volume interaction into the inlet structure associated to the highly accelerated flow, returning a minor flow discharge difference (8%).

Comparatively to Silva (2013), a better approach for the transversal jet dispersion is noticeable. However, air entrainment model had not a significant influence in flow velocities, which did not influence the maximum jet reach.

The alternative outlet structures resulted in a better option for the free jet impingement into the river valley, which contributed for reduced scour hole depths.

References

- AQUALOGUS. (2011). Barragem de salamonde: Descarregador de cheias complementar - projecto. *AQUALOGUS, Engenharia E Ambiente Lda, Volume i*-(memória descritiva e justificativa).
- Chanson, H. (2001). *The Hydraulics of Open Channel Flow: An Introduction*. (H. Chanson, Ed.)*Journal of Hydraulic Engineering* (Second Edi, Vol. 127). Oxford: Butterworth-Heinemann, Elsevier. [http://doi.org/10.1061/\(ASCE\)0733-9429\(2001\)127:3\(246\)](http://doi.org/10.1061/(ASCE)0733-9429(2001)127:3(246))
- Flow Science, I. (2014). *FLOW-3D User Manual*.
- Hirt, C. W. (2007). Scale Analysis of Two-Fluid Relative Velocity Equation: (Evaluation of Drift-Flux Approximation). *Flow Science, Inc., FSI-07-TN7*(November), 1–5.
- Silva, M. R. (2013). *Modelação numérica 3D de escoamentos em descarregadores de cheias com escoamento em superfície livre . Descarregador complementar de Salamonde*. Técnico Lisboa-Universidade de Lisboa.
- Van Rijn, L. C. (1984). Sediment transport Part I Bed load transport. *Journal of Engineering Mechanics*. [http://doi.org/10.1061/\(ASCE\)0733-9429\(1984\)110:10\(1431\)](http://doi.org/10.1061/(ASCE)0733-9429(1984)110:10(1431))